Instability of a Vortex Column Due to Turbulence Generated Axial Flow

A Thesis

Presented to

the Faculty of the Department of Mechanical Engineering

University of Houston

In Partial Fulfillment

of the Requirements for the Degree

Masters of Science

in Mechanical Engineering

by

Eric Stout

December 2013

Instability of a Vortex Column Due to Turbulence Generated Axial Flow

_____

Eric Stout

Approved:

_____

Chairman of the Committee
Fazle Hussain, Professor
Mechanical Engineering

Committee Members:

_____

Ralph Metcalfe, Professor
Mechanical Engineering

_____

Gemunu Gunaratne, Chairman
Physics

_____

Suresh Khator, Associate Dean
Cullen College of Engineering

_____

Pradeep Sharma, Chairman
Mechanical Engineering

Instability of a Vortex Column Due to Turbulence Generated Axial Flow

An Abstract

of a

Thesis

Presented to

the Faculty of the Department of Mechanical Engineering

University of Houston

In Partial Fulfillment

of the Requirements for the Degree

Masters of Science

in Mechanical Engineering

by

Eric Stout

December 2013

Abstract

Axial flow generated by turbulence on an initially two-dimensional vortex column, the Lamb-Oseen vortex, is studied theoretically and by direct numerical simulation of the Navier-Stokes equations. Azimuthally wrapped filaments of opposite circulations, discussed for the case of two oppositely oriented filaments, advect radially in opposite directions, leading to radial separation of the filaments and net axial flow on the vortex axis. Axial velocity is found to grow as $t^{5/2}$ from the simulation results, closely matching the analytically determined growth rate. Derivation of the axial flow magnitude predicts the onset of instability due to axial flow via the q (≡peak azimuthal velocity/peak axial velocity) criterion. Simulation results show (limited) renewed growth when q decreases below the unstable limit, likely dominating the previously discussed parent-offspring hairpin vortex mechanism for regenerative growth and suggesting possible breakup of the initially normal mode stable vortex at higher vortex Reynolds number due to ambient turbulence.

Table of Contents

List of Figures

Chapter 1: Introduction

Large-scale vortical motions known as *coherent structures* (CS) are now assumed to be present in turbulent shear flows, dominating flow dynamics such as momentum and energy transports, drag, heat transfer and aerodynamic noise generation. Additionally, the presence of CS enable control of turbulent shear flow through the interaction of CS with the ambient finer scale turbulence (such as in the case of turbulent boundary layers, shown by Schoppa & Hussain 2002), prompting the claim: *no CS*, *no control* (Hussain 1986). Interest here lies in understanding the CS's response to the ambient turbulence and development of instability on the vortex column, hence possible transition to turbulence. To do this, the flow is idealized as a rectilinear column vortex embedded in homogeneous, isotropic, fine-scale turbulence.

The idealized vortex-turbulence interaction is also similar to several engineering applications, such as trailing vortices behind airplanes and blade tip vortices generated by wind turbines. The passage of lifting surfaces (wings or blades) through the generated vortices induces significant lift loss and vibrations, increasing wear and fatigue, potentially leading to catastrophic failure. A safe separation distance, currently fairly conservative (Broderick 2008) due to the empirical models used (Spalart 1998), is required for the vortices to decay to a 'safe' intensity (i.e., swirl velocity). Understanding vortex decay mechanisms, in particular triggering vortex breakup into turbulence, is vital to relaxing the separation distance and improving airport and wind farm efficiency.

An isolated rectilinear vortex column section is chosen as the idealized CS, which is free from the interactions of other similar sized structures (like reconnection or pairing)

and self-induction (coiling and uncoiling of vortex lines which generate meridional flows; Melander & Hussain 1994). Also, the section is free from the effect of strain (hence elliptic instability) from adjacent vortices; see Kerswell (2002). The Lamb-Oseen vortex (hereinafter called the Oseen vortex) is selected as the CS model. The Oseen vortex is the result of a viscously diffusing line vortex and closely approximates trailing vortices, of course without any axial flow, as is the reality in the far field. Notably, the Oseen vortex is normal-mode stable, i.e., all eigenmodes exponentially decay in time (Fabre *et al.* 2006), though perturbations can grow temporarily via transient growth (Antkowiak & Brancher 2004, hereinafter AB04; Pradeep & Hussain 2006, hereinafter PH06; Antkowiak & Brancher 2007, hereinafter AB07).

Growth of fluctuations draws interest for the possible transition of the column to turbulence, a goal in alleviating air traffic concerns as well as a topic of fundamental interest in all transitioning turbulent flows. As an idealization of the large scale CS present in vortex-turbulence interaction, breakup of these filaments into finer scale turbulence represents one sustaining mechanism for turbulent flows; the other being the amplification of fine scale turbulence by strain. Idealization of the CS as an isolated vortex then identifies the influence of turbulence on the column without strain, which generates elliptic instability (Kerswell 2002) and leads to transition.

Finite amplitude, transiently growing fluctuations on a vortex column, extracted in the linear regime, have generated significant distortions of the vortex column, potentially leading to breakup of the column (Hussain, Pradeep & Stout 2011, hereinafter HPS). Transition of the column to turbulence in this manner is termed “bypass transition” as it bypasses normal mode instability thought to trigger transition to turbulence

(discussed by Morkovin 1969 in transitioning shear layers, but equally applicable here). However, these fluctuations are also known to generate a circulation overshoot, predicted by Govindaraju & Saffman (1971), confirmed by PH10 and further studied by HS, suggesting that turbulence also leads to instability of the vortex column and a second path to turbulence (a different bypass transition where the growing perturbation causes an instability, which then generates turbulence).

A second possible instability is due to axial flow on the vortex axis, which is similar to the Batchelor (or *q*, where q is the ratio of peak azimuthal to peak axial velocities) vortex. Inviscid instability is present when q is less than 1.5 (as shown by Lessen, Singh & Paillet 1974, amongst others), while slower growing viscous instabilities are possible for q less than 2.31 (Stewartson & Brown 1985). Generation of axial flow, discussed for an axially diffusing trailing vortex by Batchelor (1964), is unclear for a rectilinear column vortex embedded in turbulence. Note that any turbulent generation of axial flow is independent of the generation of axial flow due to the axial pressure gradient generated by viscous diffusion of the core in realistic (i.e., non-rectilinear) trailing vortices (Batchelor 1964).

Here the mechanism for generation of axial flow is determined both from analysis of the Reynolds averaged and from the physical evolution of the turbulent field. Then, the implications of axial flow are considered, including whether axial flow is generated on a turbulent vortex column and whether the axial flow leads to instability.

Chapter 2: Methods

The velocity (u, v, w) and vorticity $\boldsymbol{\omega}$ = (ω_r, ω_θ, ω_z) components are studied in cylindrical coordinates (r, θ, z), as shown in figure 1. The Cartesian coordinates (x, y, z), used for Fourier transforms (to avoid singularity issues at the axis for the cylindrical coordinates), are also shown. Uppercases denote mean quantities - averaged over all θ and z at each time - like mean azimuthal velocity, V, and mean axial vorticity, Ω_z, while primes, e.g., ω'_r, denote fluctuation quantities. Perturbation energy, $E = .5\int(u'^2+v'^2+w'^2)\mathrm{d}U$, is normalized by the computational volume (U). The average of a quantity over θ and z is denoted by an over-bar, e.g., $\overline{u'v'}$. The vortex Reynolds number, $Re \equiv$ circulation/viscosity$=\Gamma_\infty/\nu$, studied herein ranges from *500* to *12500*, where the column circulation (Γ_∞) is that at infinite radius – area integral of axial vorticity in a plane perpendicular to the column axis.

The simulation method uses a highly accurate pseudospectral method to correctly simulate an isolated vortex column (detailed in Pradeep & Hussain 2004). The flow is assumed to be periodic in the axial direction and is unbounded in the radial direction.

The model vortex is an Oseen vortex with mean axial vorticity:

$$\Omega_z = \Omega_0 \exp(-(r/r_1)^2), \qquad (1)$$

where Ω_0=2 is the peak mean axial vorticity and r_1=1 is the initial radius describing the core; this profile has a peak azimuthal velocity, V_0, of 0.63, a core radius, r_0, of 1.12, and a turnover time $T'=2\pi r_0/V_0$, of 11, where the turnover time is the time it takes a fluid particle at the core radius to circle the core once. Time is nondimensionalized by the turnover time as $T=t/T'$.

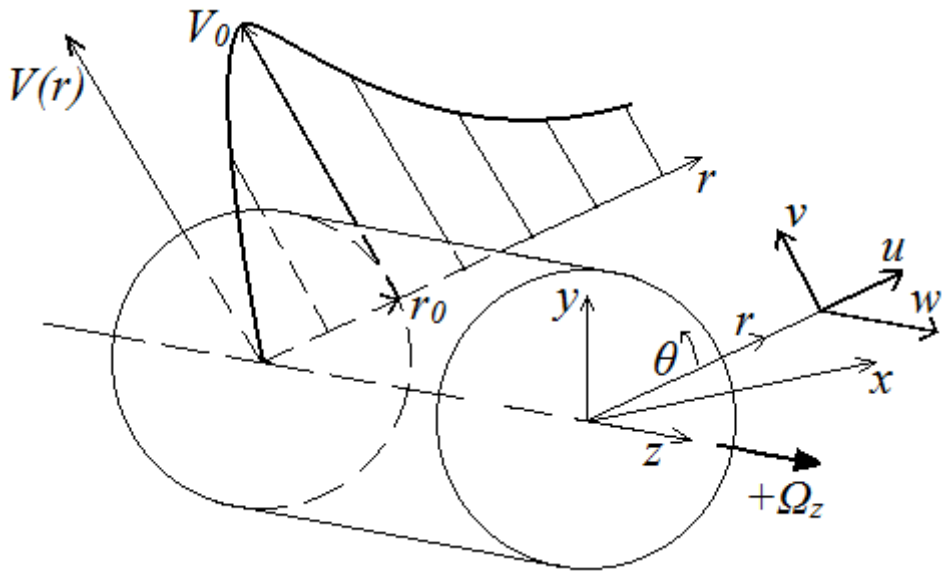

Figure 1: Velocity components (u, v, w) in cylindrical (r, θ, z) coordinates, and the mean velocity profile, $V(r)$; (x, y, z) are Cartesian coordinates. The core radius, r_0, denotes the radius of V_0, the maximum of V. Note that core vorticity, $+\Omega_z$, is in +z direction.

The turbulence is a random fluctuation field generated using the Mansour & Wray (1994) spectrum, with an initial amplitude, $\hat{u}^2(=\int(u'^2+v'^2+w'^2)\mathrm{d}\mathcal{U}$, normalized by V_0, where $\mathcal{U}$ is volume of the computational domain) of ~20%. The large initial amplitude is chosen so that the fluctuations survive the initial dissipation and evolve into late time. The particular perturbation used to idealize the axial flow mechanism is a helical (azimuthal wavenumber m=1) transient growth mode, determined using the method detailed in PH06. The initial amplitude is approximately 8%. The computational domain and mesh sizes for the turbulent case are $10\sqrt{2}\times10\sqrt{2}\times14\pi$ and 192×192×512; the domain and mesh sizes for the particular case are $10\sqrt{2}\times10\sqrt{2}\times2\pi/1.4$ and 384×384×128.

Chapter 3: Motivation

To explore the development of instabilities during vortex-turbulence interaction, consider a simulation of the Oseen vortex embedded in fine-scale turbulence at *Re*=12 500. The dynamics of vortex-turbulence interaction are briefly reviewed (discussed at length in PH10), culminating with evidence that the turbulent field alters the mean flow.

The initial turbulent vorticity field is wrapped by the mean swirl around the column axis, forming azimuthally wrapped vorticity filaments (PH10). Over time, the wrapped filaments undergo pairing into larger filaments and self-advect axially, eventually forming dipoles with oppositely oriented filaments. These filament dipoles experience enhanced cross-annihilation and eventually die out, leaving only a few filaments which did not form dipoles.

Concurrent with the generation of the filaments, mean axial flow (*W*) is found to develop throughout the evolution of vortex-turbulence interaction, shown in the *W* profiles (figure 2). The initial axial velocity is assumed to be zero everywhere. Generation of mean axial flow means that the turbulent fluctuations intensify such the initially equal magnitudes of positive and negative perturbation azimuthal vorticity (ω'_θ) at each radius become unequal, either by a difference in generation or by radial advection of azimuthally oriented filament (i.e., ω'_θ dominated filaments). The evolution of the largest (magnitude) axial flow, W_{max}, at each time (figure 3) indicates that there are two general periods for the generation of axial flow, an initial developmental period and a steadier late time period. As the initial turbulence is wrapped to form vorticity filaments

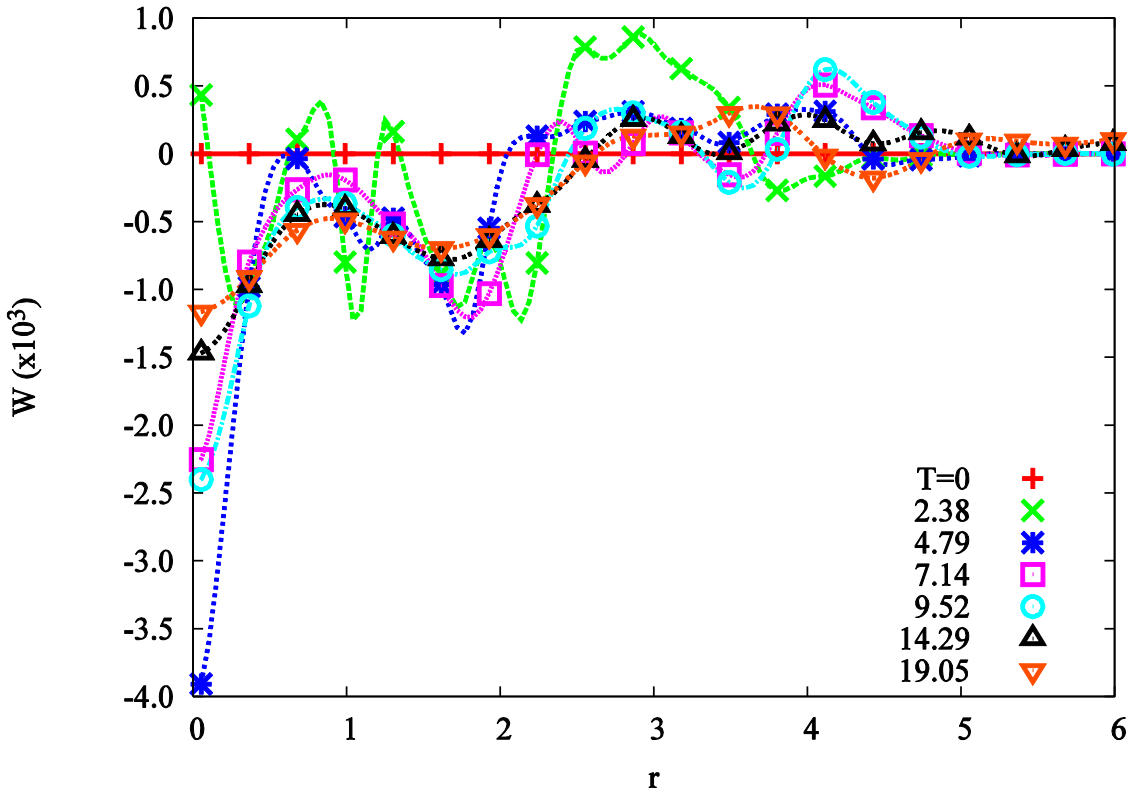

Figure 2: Profiles of mean axial velocity, W, at seven times for vortex-turbulence interaction at Re=12 500; note that $W(T=0)=0$. W is approximately 100 times smaller than the W generated for the particular case (figure 10).

via mean straining (PH10), the axial flow unsteadily increases in magnitude (though negative due the generation mechanism, discussed below). These fluctuations are due to topological changes of the filaments such as filament pairing of adjacent, same-signed filaments and viscous cross-annihilation of adjacent oppositely oriented filaments. After this initial period (T>8), W_{max} slowly decreases over time as the filaments generating axial flow viscously diffuse and cross-annihilate.

Studies of vortex-turbulence interaction have focused on the self-induced axial advection of vorticity filaments due to the azimuthal wrapping of the filaments and the radial advection due to mutual induction of a filament dipole (PH10). By approximating

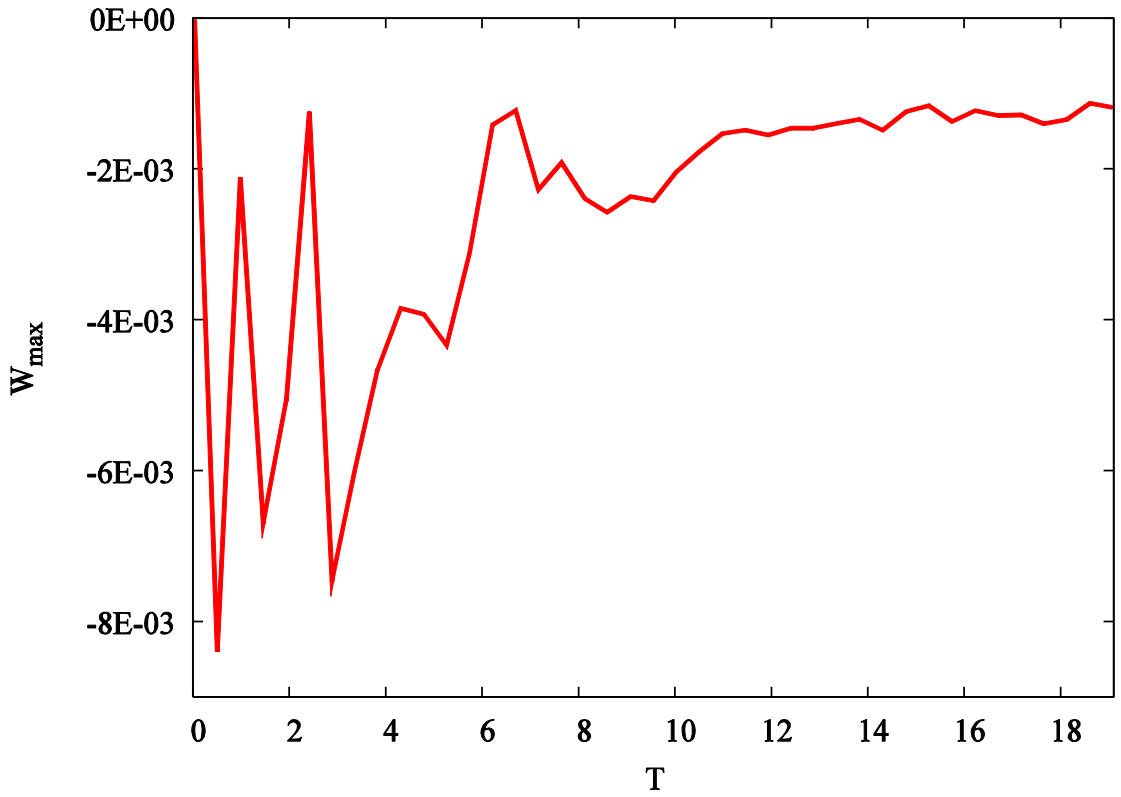

Figure 3: Evolution of peak mean axial velocity, W_{max}, for vortex-turbulence interaction at Re=12 500; note that $W(T=0)=0$. W_{max} is approximately 100 times smaller than the W_{max} generated for the particular case (figure 11).

the vorticity filaments as vortex rings to understand such motion, the effect of the radial and axial components of the filament is ignored, especially for the self-induced motion of the filaments. Note that the axial component of the vorticity filament (i.e., axial perturbation vorticity, ω'_z, plus the mean axial vorticity, Ω_z) plays no role in the vorticity generation due to mean strain. The radial component of the self-induced motion of filaments, related to the radial and axial extent of the filament, is found to drive the generation of axial flow.

Chapter 4: Theory

As a preface, the axial Reynolds-averaged Navier-Stokes equation,

$$\frac{\partial W}{\partial t}+U\frac{\partial W}{\partial r}=-\frac{1}{r}\frac{\partial r\overline{u'w'}}{\partial r}+\nu\frac{1}{r}\frac{\partial}{\partial r}\left(r\frac{\partial W}{\partial r}\right), \qquad (2)$$

show that W develops due to the $\overline{u'w'}$ generated by a vorticity filament (shown in figures 4a-b). Growth of u' is physically due to the tilting of radial perturbation vorticity into the azimuthal direction, i.e., mean shearing of the vorticity field, and thus there $\overline{u'w'}$ increases. Note that, unlike $\overline{u'v'}$ associated with energy growth, there is no coupling between u' and w' generation except through continuity ($\nabla\cdot\vec{u}=0$). The physical structure of the filament then dictates the sign of $\overline{u'w'}$ generated, not a physical phenomenon such as mean straining of the filament. Vorticity filaments then generate axial flow until limitation by viscous diffusion or nonlinear effects, such as self-induced tilting. Hence, axial flow is due to azimuthally wrapped filaments with radial and axial components; the physical mechanism for axial flow is discussed next.

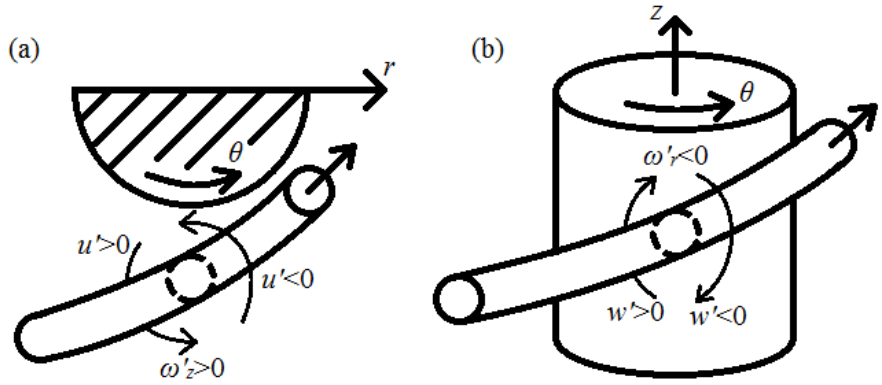

Figure 4: Example filament generating $\overline{u'w'}>0$ with (a) $\omega'_z>0$, associated with u', and (b) $\omega'_r<0$, associated with w'. Note that ω'_r and ω'_z are not linked by mean strain, which means any combination of signs is possible (i.e., $\omega'_r>0$ and $\omega'_z>0$ or vice-versa).

Chapter 5: Physical Mechanism

Jet-like axial flow (like that seen in figure 2) is intrinsically linked to mean azimuthal vorticity (Ω_θ), which arises when initially equal magnitudes of perturbation azimuthal vorticity, ω'_θ, become unequal. For this to occur, either the generation of oppositely signed ω'_θ must become different (resulting in a difference between the magnitudes of $\omega'_\theta>0$ and $\omega'_\theta<0$) or filaments of oppositely signed ω'_θ advect radially in opposite directions, resulting in radial separation of ω'_θ. However, changes to the generation of ω'_θ would result in the generation of meridional circulation, which is initially zero, resulting in a violation of conservation of circulation. On the other hand, radial advection of filaments is a spatial reorganization of the turbulent field with regions of oppositely oriented axial flow developing (discussed further later), maintaining meridional circulation at zero. Radial advection, as briefly mentioned above, is expected of the azimuthally wrapped filaments by the self-induced motion of the filament.

The self-induced motion of the filament is given by

$$\boldsymbol{u}_s(\mathbf{x})=\gamma\kappa/(4\pi)\ln(L/a)\mathbf{b}, \qquad (3)$$

where γ is the filament's circulation, κ is the curvature of the filament (i.e., the inverse of the radius of curvature), L is the length of the filament segment considered and a is the core radius of the filament, where $\ln(L/a)=A$ is assumed to be constant (Callegari and Ting 1978, Ting and Klein 1991). The two controlling factors for the direction of self-induced advection are γ, which for oppositely oriented filaments would be oppositely signed, and $\mathbf{b}$, which is determined by the curve $\mathbf{x}(\tau)$ and would be the same for

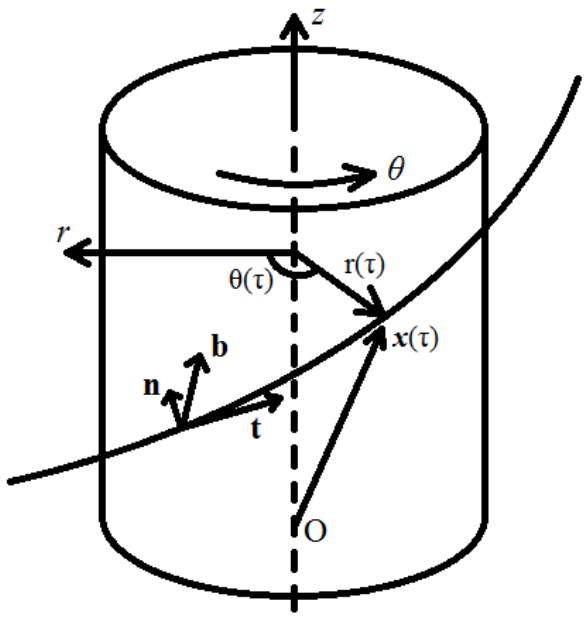

Figure 5: Vortex filament segment defined by $x(\tau) = r(\tau)\mathbf{r}+z(\tau)\mathbf{z}$ with respect to the origin *O* sketched with tangent (**t**), normal (**n**) and binormal (**b**) unit vectors shown.

oppositely oriented filaments since $\mathbf{x}(\tau)$ is determined by the orientation of the curve and not its circulation. Note that **b** and curvature are independent of γ, and are the same for filaments with opposite circulation.

To determine the binormal vector (**b**), take $\mathbf{x}(\tau) = r(\tau)\mathbf{r}+ z(\tau)\mathbf{z}$, where **r** depends on $r(\tau)$ and $\theta(\tau)$, as shown in figure 5, and expand each term: $r(\tau)=r_0+\Delta r\tau+O(\tau^2)$, $\theta(\tau)=\theta_0+\Delta\theta\tau+O(\tau^2)$ and $z(\tau)=z_0+\Delta z\tau+O(\tau^2)$, where (r_0, θ_0, z_0) are the initial position of the filament relative to the origin O, and $(\Delta r, \Delta\theta, \Delta z)$ are the first order variations of the filament curve (shown in figures 7a-c). Note that the due to the radial variation of the mean azimuthal velocity, *V*, the radial extent of the filament Δr results in an additional azimuthal wrapping of the filament around the column $\Delta\theta_s=S\Delta rt$, where S is the mean strain rate (sketched in figure 6), in addition to the initial $\Delta\theta$, $\Delta\theta_0$; hence $\Delta\theta=\Delta\theta_0+ \Delta\theta_s$. Note that S is negative and thus $\Delta\theta_s$ is oppositely signed to Δr, just like the relation

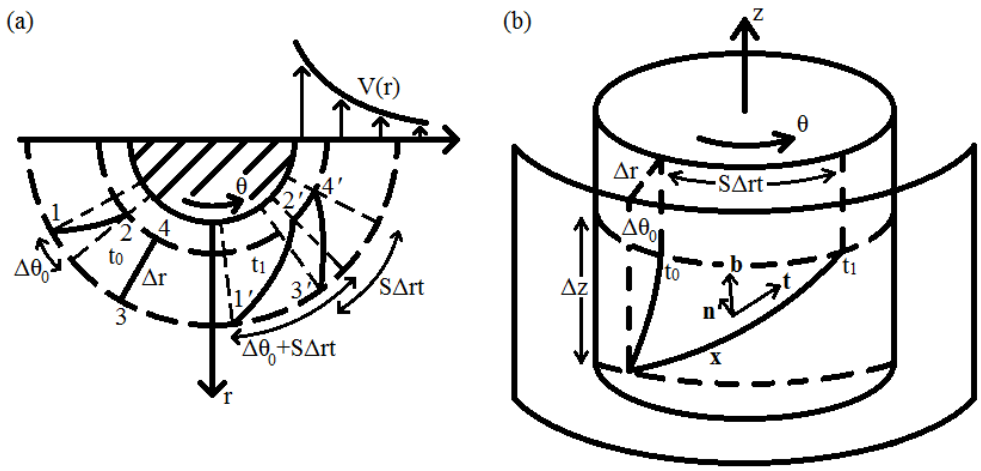

Figure 6: Effect of mean strain on vorticity filaments shown in (a) an end view and (b) an oblique view. Also shown in (b) are (**t**, **n**, **b**) and the axial extent of the filament (Δz).

between radial perturbation vorticity and mean strain generated azimuthal perturbation vorticity (PH06).

Defining **x**(τ) at each point along it are the triad of unit vectors: the tangent vector **t**, which points in the direction of the filament or in the direction that **x**(τ) varies; the normal vector, which points towards the center of curvature for the filament; and the binormal vector, which is **t**×**n** and forms a right-handed set of vectors with the tangent and binormal (sketched in figure 5). Physically, **b** is the normal vector for the plane defined by **t** and **n**, and is angled with respect to the column axis for the curve **x**(τ). For example, the tangent vector **t** for a vortex ring is in the azimuthal direction, **n** points towards the vortex axis (–**r** direction) and **b** is in the axial direction, depending on the direction of **t**. With the addition of axial dependence, i.e., for a helical vortex line, **t** has azimuthal and axial components, **n** remains unchanged, and **b** has azimuthal and axial components. Finally, for a filament with radial, azimuthal and axial variations, as described above, each unit vector (**t**, **n**, **b**) has components in (**r**, **θ**, **z**), as shown in figure 7.

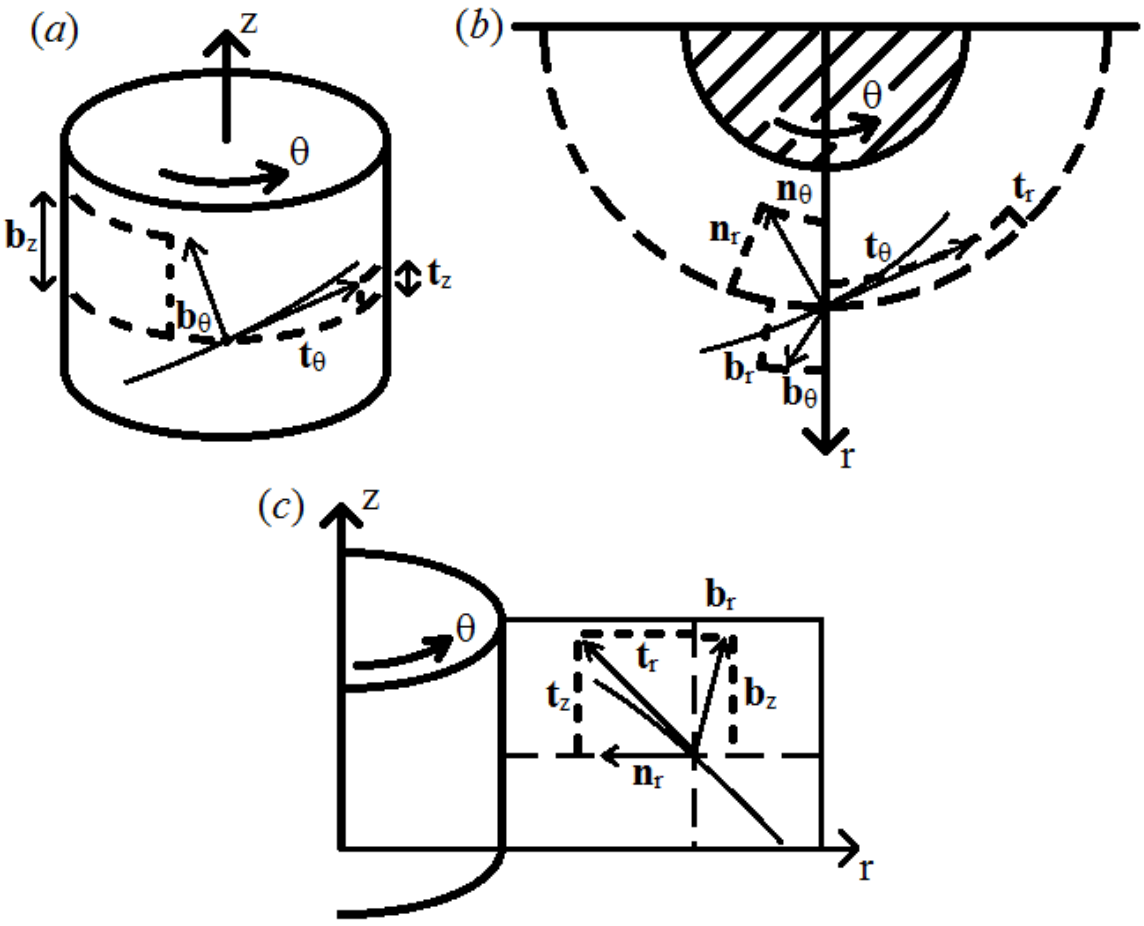

Figure 7: Decomposition of **t**, **n** and **b** in (a) a θ-z plane (a cylinder coaxial with the vortex column); (b) in an r-θ plane (looking down the z axis); and (c) in an r-z plane. Note that **n** lies in the r-θ plane, with $\mathbf{n_\theta}$ omitted from (a) for clarity.

Calculating **n** from $\mathbf{x}(\tau)$, its second derivative, gives the curvature $\kappa \sim [r_c(S\Delta rt)^2]^{-1}$, where r_c is the initial radius of the filament. Deriving the three components of **b** using **t** and **n** (the individual components of (**t**, **n**, **b**) are sketched in figure 7) gives

$$\mathbf{b}\cdot\mathbf{r} = -\Delta r \Delta z (S\Delta rt)/|\mathbf{b}|, \tag{4.1}$$

$$\mathbf{b}\cdot\boldsymbol{\theta} = (r_c+\Delta r\tau)(S\Delta rt)^2\Delta z/|\mathbf{b}|, \text{ and} \tag{4.2}$$

$$\mathbf{b}\cdot\mathbf{z} = [2\Delta r^2(\theta_0+S\Delta rt\tau)-(r_c+\Delta r\tau)^2\Delta\theta^3]/|\mathbf{b}|, \tag{4.3}$$

where $|\mathbf{b}| \approx r_c^2(S\Delta rt)^3$, based on order of magnitude approximations. From (4.1), the self-

induced radial velocity of the filament, (3), then becomes

$$\boldsymbol{u_s}\cdot\mathbf{r} = \gamma A \Delta z \Delta r/[2\pi r_c^3 (S\Delta rt)^4], \quad (5)$$

where $\Delta\theta_0$ is assumed to be negligible compared to the mean straining term.

Integration of (5) in time and expanding the t^{-3} term gives

$$r_f \approx r_c + \gamma A \Delta r \Delta z t^3/[6\pi r_c^3 (S\Delta rt_0)^4], \quad (6)$$

indicating a cubic dependence in time for the radial shift of the filament, where t_0 is an artificial origin such that r_f=0 at t=0. To illustrate this, consider a space curve, $\mathbf{x}(\tau)$, as shown in figure 8(a). For a filament with γ>0 (figure 8b, top filament), the filament radially advects outward (as well as in the +z direction) from t_0 to t_1, as expected from eqn. (6); similarly, a filament with γ<0 (figure 8b, bottom filament) radially advects inward (and in the $-\mathbf{z}$ direction).

Note that Δz is assumed to be positive, as the mean axial vorticity, Ω_z, is positive outside the core for the Oseen vortex. However, there are instances, such as outside a Rankine vortex, where Ω_z=0 and the space curve is described by the fluctuation axial vorticity ω'_z, and for a circulation overshoot, where Ω_z is negative, that Δz may be negative.

The axial velocity induced by the filament (approximated as a ring), W_f, is given by

$$W_f = \gamma/(2r_f). \quad (7)$$

Inserting r_f, eqn. (6), into eqn. (7) gives

$$W_f \approx \gamma/\{2r_c + \gamma A \Delta r \Delta z t^3/[6\pi r_c^3 (S\Delta rt_0)^4]\}. \quad (8)$$

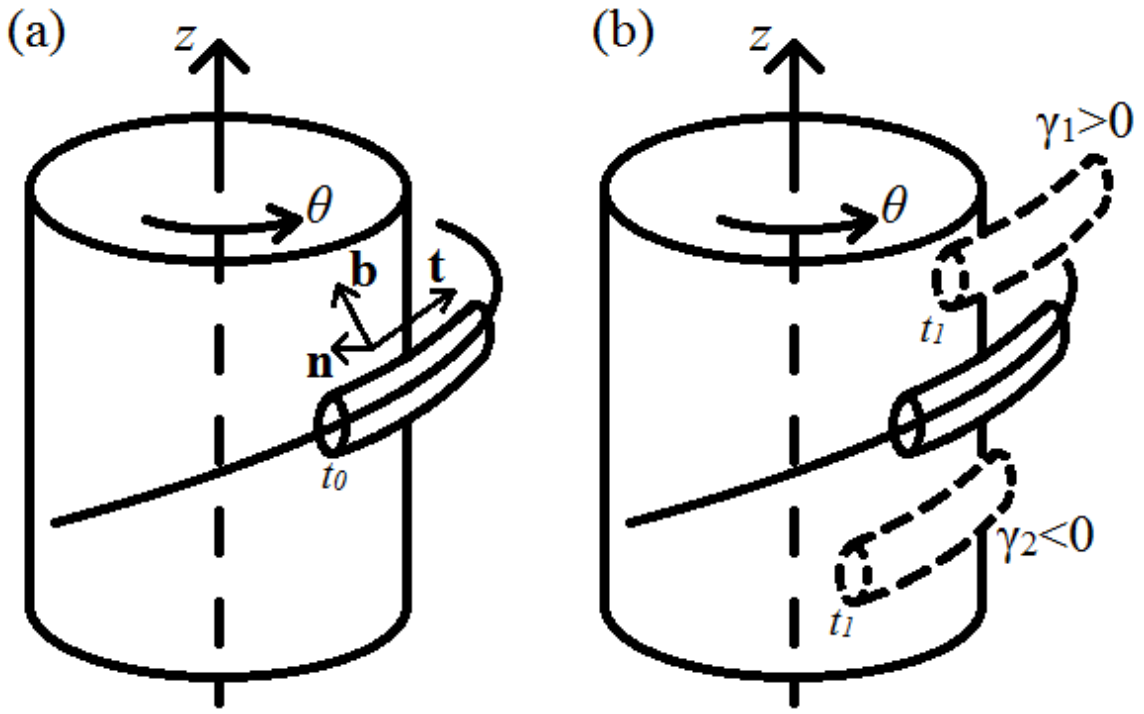

Figure 8: (a) Vorticity filament segment with $\Delta r<0$ and $\Delta z>0$ at t_0 with (**t**, **n**, **b**) shown. Note that **b** is in (+*r*, +*z*) direction. (b) Advection of a filament at t_1 with $\gamma_1>0$ (upper), in the direction of the binormal, and $\gamma_2<0$ (lower), in the opposite direction of the binormal.

Two oppositely oriented filaments, with circulations $\gamma_1=C\Gamma$ and $\gamma_2=-C\Gamma$ where C is the ratio between the filaments' individual circulation to the column's circulation, the total induced axial velocity of the two filaments, W_{f1} and W_{f2}, is

$$W_{tot}=-\gamma^2 A\Delta r\Delta z t^3/[6\pi r_c^5(S\Delta r t_0)^4]. \quad (9)$$

The effects of strain, seen in the curvature and binormal vector, would dominate the growth of W_{tot} at early times; note the cubic rate matches the linear analysis extended from Pradeep & Hussain (2006). As nonlinear effects influence the filament evolution (discussed later), the cubic growth ends and the linear in time term dominates growth of W_{tot}, which matches the trends in the simulations, discussed later (§6, figure 12).

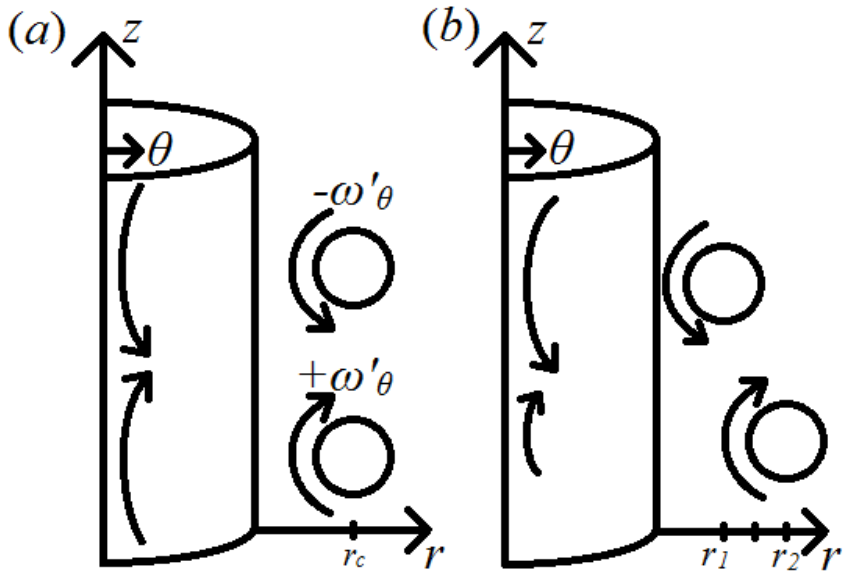

Figure 9: (*a*) Cross sectional sketch of two oppositely oriented filaments with $+\omega'_\theta$ and $-\omega'_\theta$ at the same radius, r_c, and their induced flows at the axis. (*b*) Filaments' positions at a later time, resulting in a net axial flow (the difference between the two arrows).

Note that eqn. (6) for filaments with (oppositely signed) γ_1 and γ_2 (with $\Delta r<0$ and $\Delta z>0$, as shown in figure 8) gives opposite changed to r_f due to the opposite sign of γ (as shown in figure 9 where azimuthal vorticity, ω'_θ, indicates the circulation), hence W generated by filament 1 (with positive γ and radial advection outward, shown between figures 7b-c) would decrease, and W generated by filament 2 would increase. Furthermore, the direction of each W_f is entirely contained within the first two terms of the right hand side of (8), which means the net direction of W_{tot} must be determined by which filament is closer to the axis (hence stronger W_f generated). From (6), the filament with $\gamma=-C\Gamma$ (i.e., filament 2) moves closer to the column and gives the direction of W_{tot} as negative. Physically, the self-induced velocity of the filaments leads to filaments initially at the same radius moving radially apart, generating a mean axial flow on the axis.

A second physical interpretation can be derived from helical wave decomposition (Melander & Hussain 1993). From analysis of the vorticity field in MH93, right-handed

vorticity tends to be dominated by vorticity filaments with positive azimuthal vorticity (ω'_θ>0) while left-handed filaments are dominated by ω'_θ<0. Note that right-handed vorticity naturally generates left-handed vorticity, and vice-versa, so no filament is ever purely in a single handed direction. The self-evolution of a polarized vorticity field is found to be one of the driving factors for the polarized vorticity field evolution, on par with the transport due to the opposite polarity vorticity field; in the case of a filament dominated by a single polarity where the opposite polarity vorticity is negligible, self-induced motion of the polarized vorticity dominates. If sections of these filaments are idealized as sections of circular vorticity filaments, their self-induced velocities are in opposite directions, leading to radial separation, as discussed before. The result of this self-induced motion is a polarization of the vorticity field, with alternating layers of left- and right-handed vorticity coaxial with the vortex core. Since axial flow on a vortex column, for instance in a Batchelor vortex, is due to polarized vortex lines, layering of polarized (fluctuation) vorticity fields outside the core naturally leads to axial flow.

The assumptions made in the derivation of eqn. (9) are briefly discussed here. First, in determining the tangent, normal and binormal unit vectors to the filament, the mean strain, S, is assumed to be a constant for the segment of the filament. Since $S \sim r^{-3}$ in the potential region outside the vortex column and the radial variation (Δr) and radial shift, the second term in (6), are small, this is a valid assumption until the radial shift becomes significant. Additionally, movement of the filament radially inward towards the column will eventually be inhibited by the column, which acts like a deformable surface. This would accelerate the shift in the tangent towards the azimuthal direction and move

the binormal towards the axial direction, ending the radial movement of one of the filaments and slowing the generation of W_{tot}.

Also, the components of **b** (4.1-4.3) are simplified using their magnitude, and $\Delta\theta_0$ may be significant, particularly in the turbulent case. However, the assumptions hold at later times, when the mean straining term dominates the **θ** term. Finally, these assumptions hold true when the self-induced velocity is a dominant term for the total velocity of the filament, which includes the mean azimuthal velocity and the velocity generated by adjacent filaments. For a filament dipole formed from two oppositely oriented filaments, the mutually induction of the two filaments eventually dominates the self-induced motion of each individual filament, leading to radially outward advection (PH10 and others). Dipole formation limits the generation of axial flow once the mutual induction of two adjacent filaments with small (and decreasing) separation, prior to that, the self-induction dominates, leading to the differing radial advection discussed above.

Chapter 6: Results & Discussion

To validate eqn. (9), briefly consider the effects for two oppositely oriented filaments outside the column with $\gamma_1 = 0.1\Gamma$ and $\gamma_2 = 0.1\Gamma$ at a radius of $r_c = 1.5r_0$ and a segment with radial and axial length $\Delta r = \Delta z = 0.01r_0$, where r_0=1 is the vortex core radius. As the filament is outside the core, $S \approx -\Gamma r_c^{-2}$.

Evaluate t_0 and insert into eqn. (9), $W_{tot} \approx \gamma^2 A\Delta r\Delta z t^3/[6\pi\, r_c^5 (S\Delta r t_0)^4]$; let t_0=T, to account for the initial wrapping of the filament, and A = ln(L/a)~10, i.e., the filament length is much longer than the filament's core radius due to the mean straining effect. Taking Γ=1, $W_{tot}(t=1)$=0.0122 and $W_{tot}(t=2)$=0.0978, after which the assumption of small radial separation no longer holds though axial flow continues to be generated. Since $V_{max}=\Gamma/r_0=1$, $q=V_{max}/W_{max}$, where $W_{max}=W_{tot}$, has dropped from infinity to 10.2 at t=2, with q continuing to decrease towards 1.5, the unstable value. Note that t_0, A, and γ are estimated (with γ based on the observed values in PH10). Viscous effects, which would eventually limit the filaments' self-induced radial advection and the generation of axial flow by diffusing the filaments, limit the decrease in q.

The above analysis assumes two thin cored vortex filaments, and that for the case of larger filaments (or multiple filaments), the value of W_{tot} would further increase, hence an even lower q. In the case of vortex turbulence interaction, θ_0 and the time it takes mean straining to dominate the structure of $\mathbf{x}(\tau)$ delays the development of W_{tot} as not all filaments begin to radially advect at the same time. Furthermore, dipole formation and viscous cross-annihilation reduces (though not completely eliminating, as seen in PH10) the number of filaments which generate axial flow over time, also limiting W_{tot} generated.

Briefly note that for axial flow to be generated, there must be a difference in the number of $\gamma>0$ filaments advected inward and the number of $\gamma<0$ filaments advected inward (and vice-versa), i.e., a different number of filament pairs spiraling upward versus spiraling downward. In the case of an infinitely long vortex column embedded in a random turbulent field, this is not possible, as there are an infinite number of filaments of either orientation (left-handed spiraling or right-handed spiraling) and either circulation. However, for a long but finite vortex, the initial turbulent field consists of a number of filaments, which can then undergo radial advection and lead to axial flow. Hence, the infinitely long vortex column would have local axial flows due to segments of the column, indicating the development of stagnation points and possible vortex breakup in the infinitely long case.

To illustrate the mechanism, consider the development of mean axial flow for a transiently growing helical (azimuthal wavenumber m=1) perturbation (PH06) at Re=10 000. The perturbation selected is the Re=5 000 transient growth optimal perturbation, which means it is the largest growing perturbation possible at Re=5 000 in the linear regime. The perturbation is selected as a long lived helical perturbation, which is due to its transient growth, not because it is a transient growth optimal perturbation. Mean straining of the perturbation generates initial growth, as discussed above for figure 6(a), before growth is limited by the effect of mean axial vorticity, i.e., core dynamics, and the perturbation viscously decays (PH06).

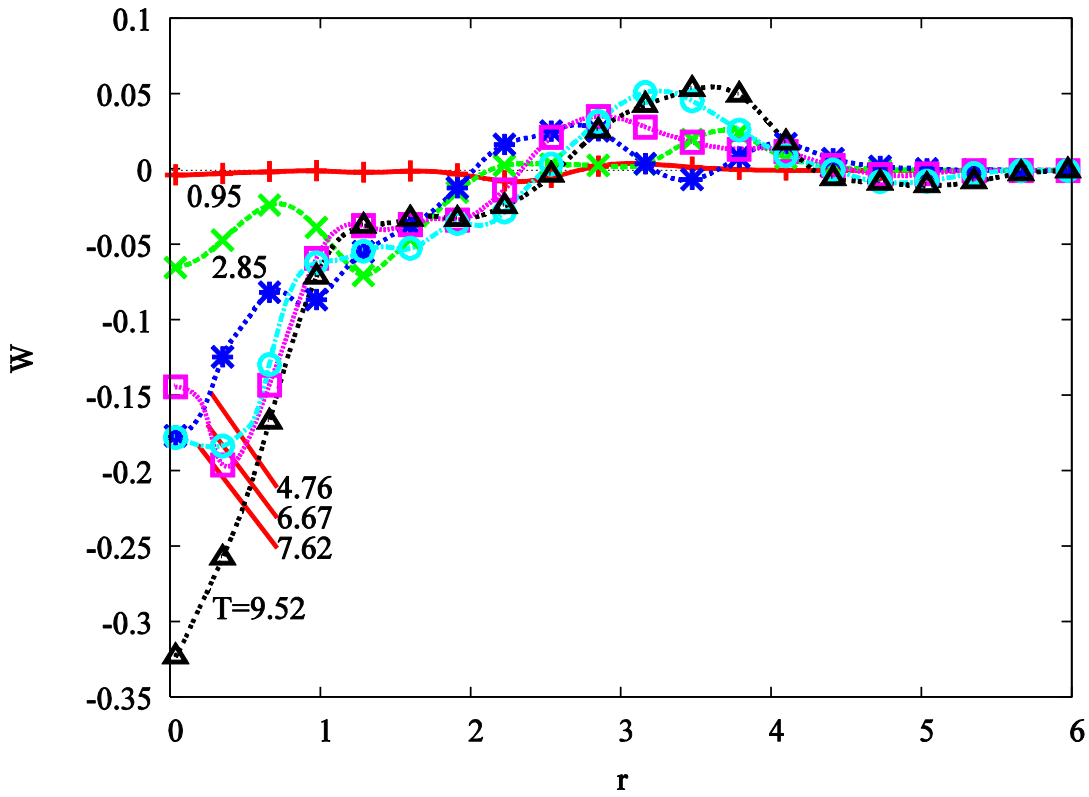

Figure 10: Profiles of W at six times for the perturbation at Re=10 000; note that W(t=0)=0, which is marked by the horizontal dotted line. Between t=50 and 100, there is a decrease in W at the axis, likely due to distortion of the axis.

Profiles of the mean axial velocity (figure 10) confirm the development of significant axial flow at the vortex axis (r=0), a result of the organization of the small scale fluctuations. Since the meridional circulation remains zero, there is a region of oppositely-oriented axial flow corresponding to layers of oppositely-oriented Ω_θ encircling the vortex axis, generated by the imbalance in the filaments' strengths radially transporting the filaments. Note that the profiles near the axis appear almost Gaussian, though, near $r\approx1.5$, the transport by the filaments distorts the profile. Continued generation of axial flow would lead to instability unstable, a topic for further research.

Note that the profiles for the m=1 perturbation and the turbulent case are similar. For example, the radius where the profile crosses W=0 for the turbulent ($r\approx2.5$, figure 2)

and m=1 (r≈2.5, figure 10) cases are approximately equal. Additionally, the Gaussian shape near the axis for the two cases are similar, though different magnitude. The similar structures mean that the profiles are likely driven by the same fundamental dynamics – transient growth of helical perturbations (discussed in HPS).

The peak axial velocity (figure 11) for the given perturbation also increases with increasing *Re*, due to decreasing viscous diffusion of the filaments driving growth. Note that $W \sim t^{5/2}$, which matches the rate predicted by eqn. (9). At late times, W grows linearly as the assumptions in the derivation of eqn. (9) no longer hold, as the assumption of small radial advection is violated. Additionally, the filaments do not undergo purely self-induced advection as additional filaments are present around the column and generate radial flow, potentially even forming a vorticity filament dipole at later times. The individual filaments are also not thin-cored, and begin to distort due to the velocity field induced by the adjacent filament, as well as their own self-induction. The late-time linear growth of W at high *Re* suggests that the generation of axial velocity does continue similar to the idealized case above, though finite filament size and mutual interaction of the filaments play an increasingly large role in W.

For the turbulence case (figure 2), the profiles drastically evolve from the early times, specifically the radial oscillations at T=2.4. These initial distortions arise from the varying concentration of fluctuation vorticity, which after mean straining, results in slightly different filament magnitudes. Over time, the stronger filament self-advection in the particular case generates greater W at the vortex axis (and the regions of oppositely oriented flow at large radii to maintain zero meridional circulation). Self-advection is clearer in the particular case (figure 10), where the initial vorticity distribution is

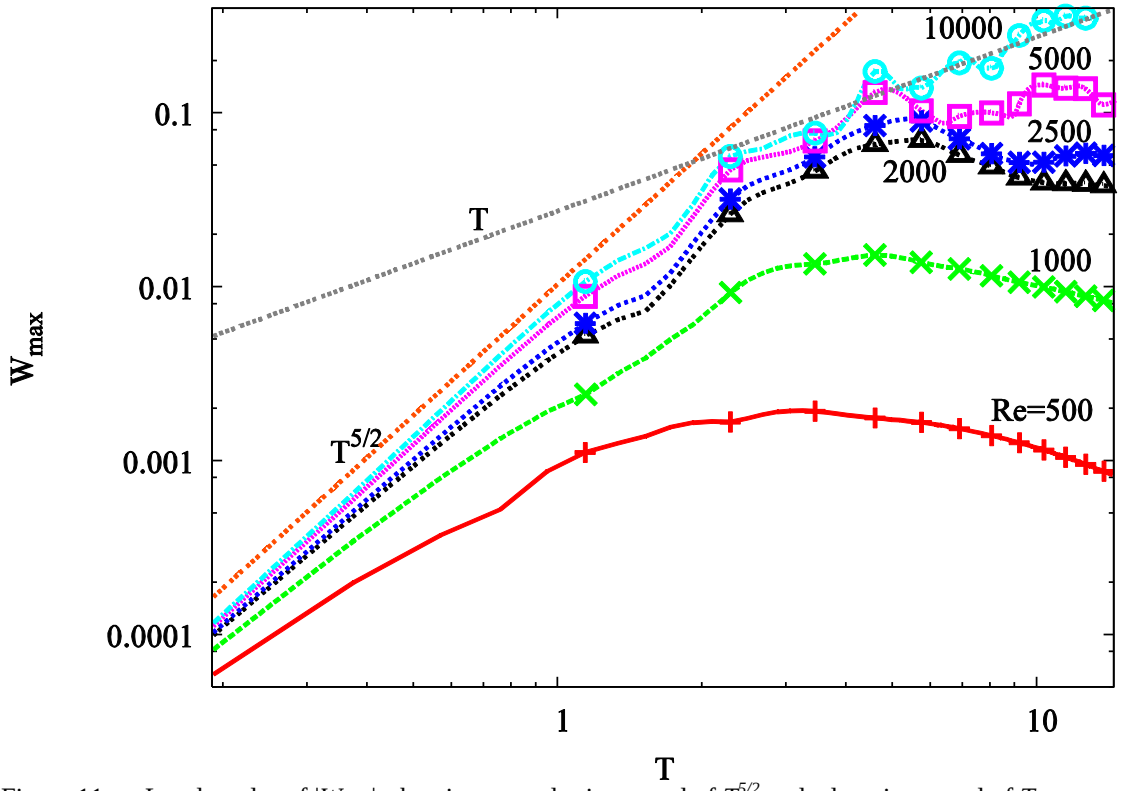

Figure 11: Log-log plot of $|W_{max}|$, showing an early time trend of $T^{5/2}$ and a late time trend of T.

localized in two oppositely oriented filaments, thus the removing random initial azimuthal amplitude in the turbulent case that is ignored in eqn. (5).

In the particular case above, the filaments are five times as strong and located at r_c=2.7r_0, thus the estimation of W_{tot} and q from eqn. (9) shows the value of q decreases below the unstable limit, confirmed in figure 12, the time evolution of q. This is notable given the axial flow in vortex-turbulence interaction, which would continue to increase at higher *Re* as the filaments last longer to generate greater *W*. Additionally, the perturbation in the particular case idealizes the structure with the largest energy found in vortex-turbulence interaction, the optimal transient growth perturbation (HPS), suggesting that at late times, the axial flow will further increase as the optimal mode comes to dominate the flow.

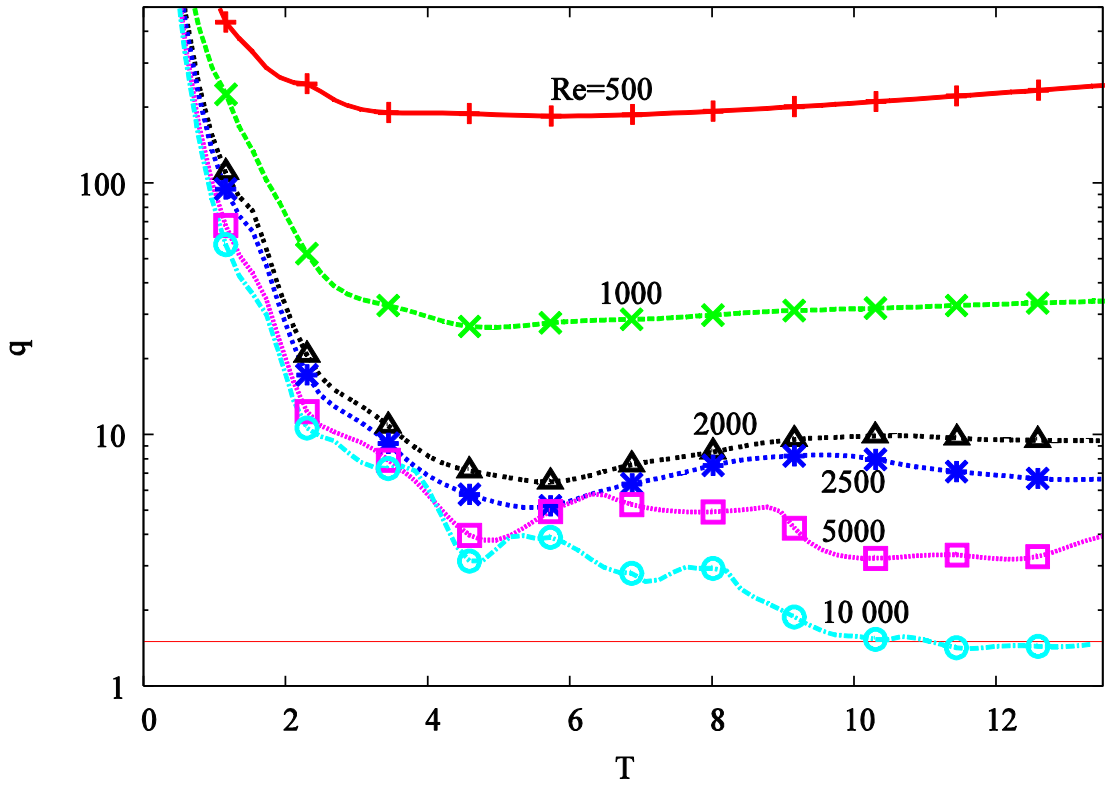

Figure 12: Evolution of $q=|V_{max}/W_{max}|$ at six *Re* (500, 1000, 2000, 2500, 5000, 10000), with q=1.5 marked by the dashed horizontal line (q<1.5 is unstable). At T=11, q<1.5, suggesting that the vortex becomes unstable.

Fluctuations in q (figure 12), especially at higher *Re*, are due to helical (azimuthal wavenumber m=1) distortion of the core, sketched in figure 13. The radial velocity induced by helical filaments outside the column at the axis radially displaces the axis. Once the axis is displaced, the cylindrical averages used here then no longer correspond with the coordinate system of the vortex column. For instance, the total flow along the helically displaced vortex axis is only partially captured by the average of the ***z*** (cylindrical coordinates) component of the velocity field. Comparing the evolution of the radial displacement (figure 14), measured by the radial position of the vorticity magnitude centroid, $\bar{r}$, taken to be the centroid of all vorticity which is above 75% of the

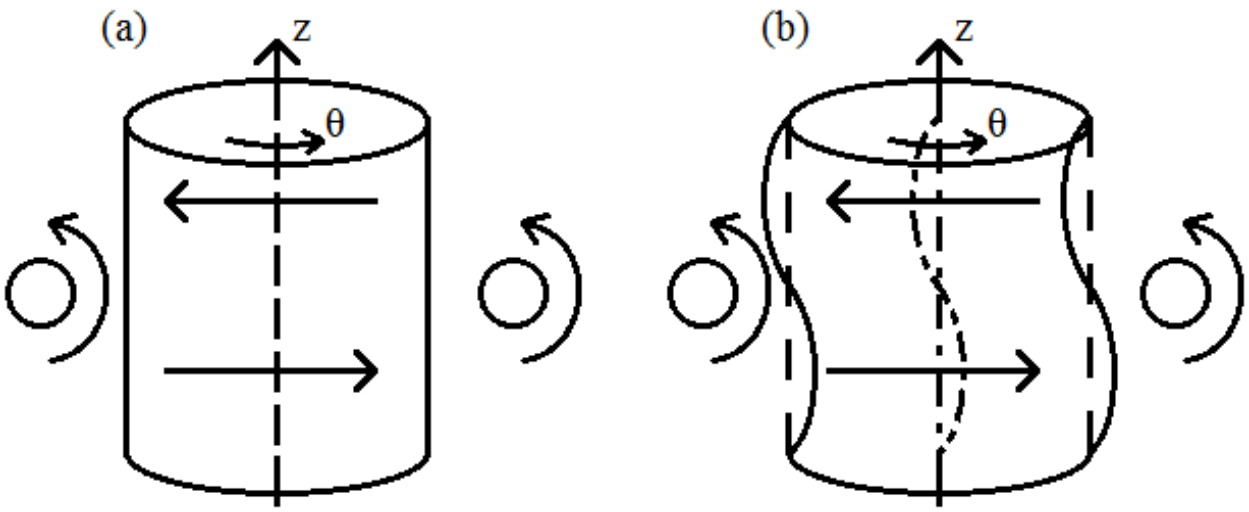

Figure 13: (a) An initially rectilinear vortex column is perturbed with a helical (m=1) perturbation. (b) The perturbation's induced velocity displaces the axis, causing the vortex to become helical.

maximum vorticity, to the evolution of q shows that the fluctuations in q correspond to increased distortion of the vortex axis. Hence, q consistently decreases towards the unstable range, even as the vortex column is distorted helically.

To investigate whether the decrease in q leads to instability and perturbation energy growth, the evolution of the volume-integrated turbulence kinetic energy, E(T)(= $0.5\int(u'^2+v'^2+w'^2)r\mathrm{d}r\mathrm{d}\theta\mathrm{d}z$, normalized by $2\pi r_l z_l$, where r_l and z_l are the radial and axial lengths of the computational domain, figure 15) is examined for energy growth when q<1.5 at T~11 (figure 12). Evolution of $E(T)$ is dominated by the initial energy growth, which increases with increasing Re, and is a result of transient growth (noted before). At Re=10 000, when q decreases below 1.5, $E(T)$ increases slightly before decreasing again, suggesting instability. Examination of the turbulent kinetic energy profiles, E(r, T) (= $0.5\int(u'^2+v'^2+w'^2)r\mathrm{d}\theta\mathrm{d}z$), for the Re=10 000 case between T≈11 and 12 show a region of energy growth between r≈0.5 and r≈1.5 (figure 16, with the region of interest shown in the inset). Note that the distortion of the vortex axis during this time is increasing, and

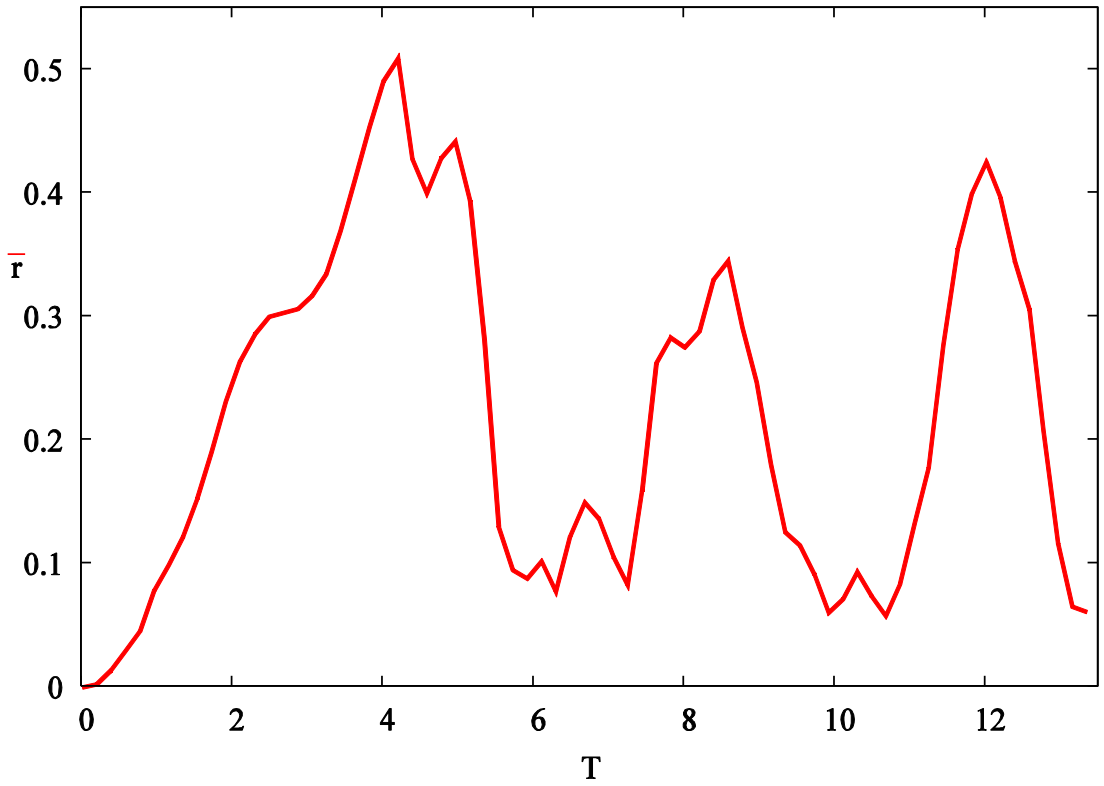

Figure 14: Evolution of the vorticity magnitude centroid relative to the initial position ($\bar{r}$) due to the helical perturbation, denoting the center of the vortex, at *Re*=10000. Fluctuations in $\bar{r}$ cause fluctuations in W_{max} (figure 11) and q (figure 12).

has an average position near r=0.5, suggesting that this growth is within and on the edge of the core. Between T=10.9 and 11.6, there is notable increase in energy at r=1, at the core edge, where $W(r)$ generates significant strain (the radial gradient of W, seen in figure 10), hence energy production. Over time, the viscous decay of W means less energy production and the onset of decay, with decay beginning at T=11.8 (figure 16). Note that the energy increase shown in the inset of figure 16 is balanced out by the decay of the energy peak at $r\approx0.25$, i.e., decay of core fluctuations.

Similar regenerative energy growth was observed in HPS, and described using a parent-offspring hairpin vortex mechanism for renewed vorticity generation and

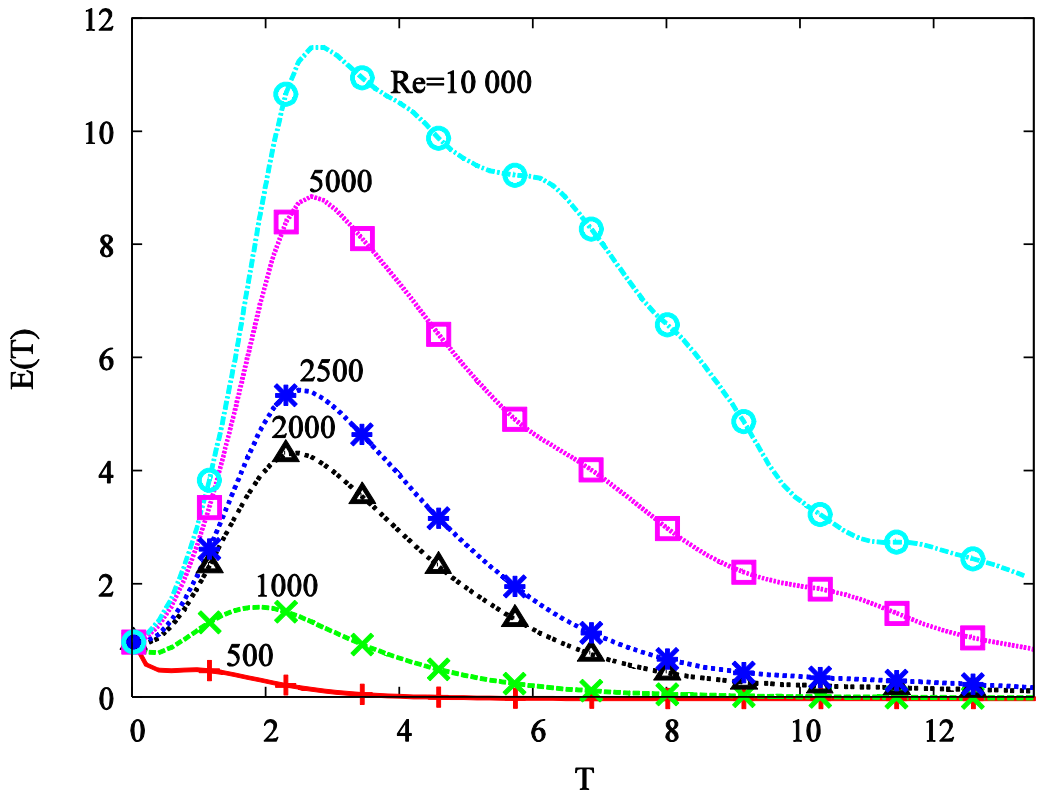

Figure 15: Evolution of the volume integrated (normalized) turbulent kinetic energy for the particular case at six *Re*. Note that at $T \approx 11$ for *Re*=10 000, the energy slightly increases, corresponding to the onset of instability in figure 12.

perturbation growth. According to HPS, a mean vortex line which has been radially perturbed (figure 17a), is wrapped azimuthally by the mean strain to generate an azimuthally oriented vorticity filament (the parent hairpin, figure 17b) which tilts axial vortex lines radially (shown as the perturbed vortex line in figure 17b). The newly perturbed vortex lines are then wrapped by the mean strain to generate a newly intensifying filament, hence renewed energy growth. To illustrate this, ω_y contours in a meridional (z-x) plane (figure 18), which corresponds to ω_θ above the axis and $-\omega_\theta$ below the axis, are shown before and during the regenerative growth period seen in figure 15.

Note that the axial flow is in the $-z$ direction (right to left). As the hairpin mechanism depends on azimuthally wrapped filaments, tilting of vortex lines occurs

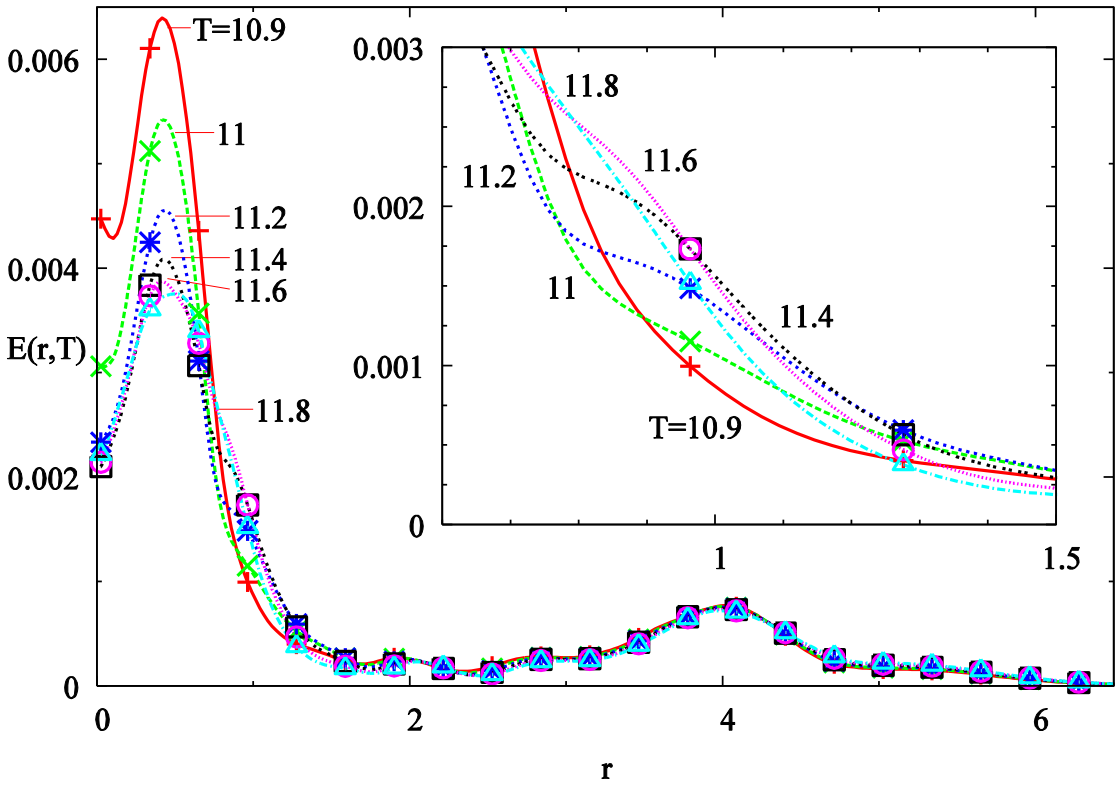

Figure 16: Profiles of TKE at six times for the *Re* = 10 000 case during the late time period of regenerative growth (from $T\approx11$ to $T\approx12$ in figure 15). Inset shows the radial region where TKE increases, then peaks (at $T\approx11.5$) and decay during this period.

throughout the evolution of the flow, and generates offspring filaments from the onset of the flow; confirmed by meridional plane contours of ω_x (figure 19; corresponding to ω_r above the axis and $-\omega_r$ below the axis) which show that the parent filament (marked by 1 in figures 18 and 19) generates ω_r radially inward. Note that the offspring vortex is generating ω_x (i.e., ω_r) at T=10.5 (figure 19a, marked by 2), before regenerative growth occurs, and these four regions (two below each leg of the hairpin, due to the tilting by each filament) remain approximately constant both in ω_x and ω_y (compare regions 1-1′′′′, the parent hairpin, and 2-2′′′′, the offspring hairpin, in figures 19 and 18 respectively). For regenerative growth to occur the tilting of vortex lines by the parent filament must exceed the diffusion of the offspring filament's vorticity, which would not occur as both the

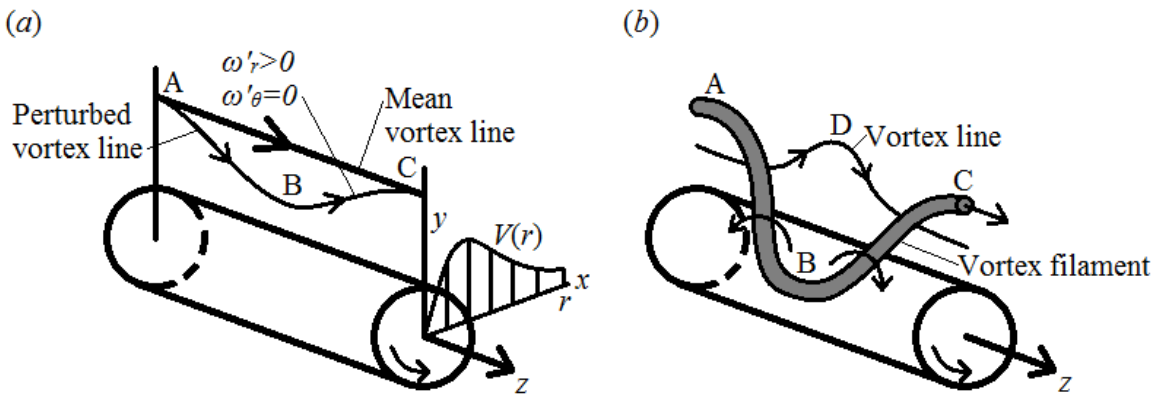

Figure 17: Postulated parent-offspring hairpin vortex mechanism from HPS.

initial and offspring filaments decay; hence the hairpin mechanism cannot result in amplification of the offspring filament at late times.

Generation of axial flow depends on the radial separation of the filaments and their circulations, and thus occurs even as the filaments decay as long as their radial separation increases. Contours of ω_y show a sheath of same-signed ω_θ around the core, as expected for the axial flow present. The region of energy growth seen in figure 16, near the core axis (confirmed by the intensifying contours near the axis in figure 18), indicates that the offspring mechanism is not the source, as the original filaments, seen at the peak near r=4, and the offspring, seen near r=2, both are unamplified during the regenerative period. Note that the filaments at r>1.5, i.e., the "parent" and "offspring" filaments from HPS, remain approximately constant. These radial locations are confirmed by the contours in figures 18(a-e), where the initial filaments have formed a dipole indicated by 1-1′′′′ in figures 18(a-e) and the offspring filaments, which are composed of oppositely signed vorticity and lie radially inwards of them, are indicated by 2-2′′′′ in figures 18(a-e). Given that the second offspring filaments (marked by 3-3′′′′) re-intensifies after decaying, while the parent filaments (in this case 2-2′′′′) also decay (hence their vorticity

production also decreases), the hairpin mechanism cannot lead to the regenerative growth.

Instead, consider the effects of a perturbation to a Batchelor vortex from the linearized perturbation vorticity equations:

$$\frac{D\omega_r'}{Dt} = \frac{\Omega_\theta}{r}\frac{\partial u'}{\partial \theta} + \Omega_z \frac{\partial u'}{\partial z},$$

$$\frac{D\omega_\theta'}{Dt} = \frac{\Omega_\theta}{r}\frac{\partial v'}{\partial \theta} + \Omega_z \frac{\partial v'}{\partial z} + S\omega_r' + \frac{u'\Omega_\theta}{r}, \text{ and} \qquad (10)$$

$$\frac{D\omega_z'}{Dt} = \frac{\Omega_\theta}{r}\frac{\partial w'}{\partial \theta} + \Omega_z \frac{\partial w'}{\partial z} + \omega_r' \frac{\partial W}{\partial r},$$

where $S=r\partial(V/r)/\partial r$ is the strain due to the mean azimuthal velocity and $D(\cdot)/Dt=\partial(\cdot)/\partial t+U\partial(\cdot)/\partial r+(V/r)\partial(\cdot)/\partial\theta+W\partial(\cdot)/\partial z$. In cases where $W(r)= \Omega_\theta(r)=0$, eqn. (10) recovers the equations for perturbations to the Oseen vortex (PH06). The additional terms, the first term on the right hand side of the three component equations and the last term for the ω'_θ and ω'_z equations, due to the mean axial flow and mean azimuthal vorticity identify the mechanism of instability for a Batchelor vortex. Mean axial flow generates ω'_z from ω'_r by $\omega'_r\partial W/\partial r$, as sketched in figure 20(a). Initially, a filament composed of purely ω'_r is tilted into ω'_z by the radial gradient of W, i.e., mean strain associated with axial velocity, producing ω'_z of opposite sign to ω'_r. Mean azimuthal vorticity has two terms: $(\Omega_\theta/r)\partial \boldsymbol{u}'/\partial\theta$, which corresponds to tilting of the mean azimuthal vorticity lines (circles concentric with the vortex core) into the radial direction; and $(u'\Omega_\theta)/r$ which is radial advection of Ω_θ by the perturbation velocity. Of these terms, generation of ω'_r by $(\Omega_\theta/r)\partial u'/\partial\theta$, closes the loop in vorticity generation necessary for instability. As sketched in figure 20(*b*), tilting of Ω_θ by u' associated with ω'_z generates

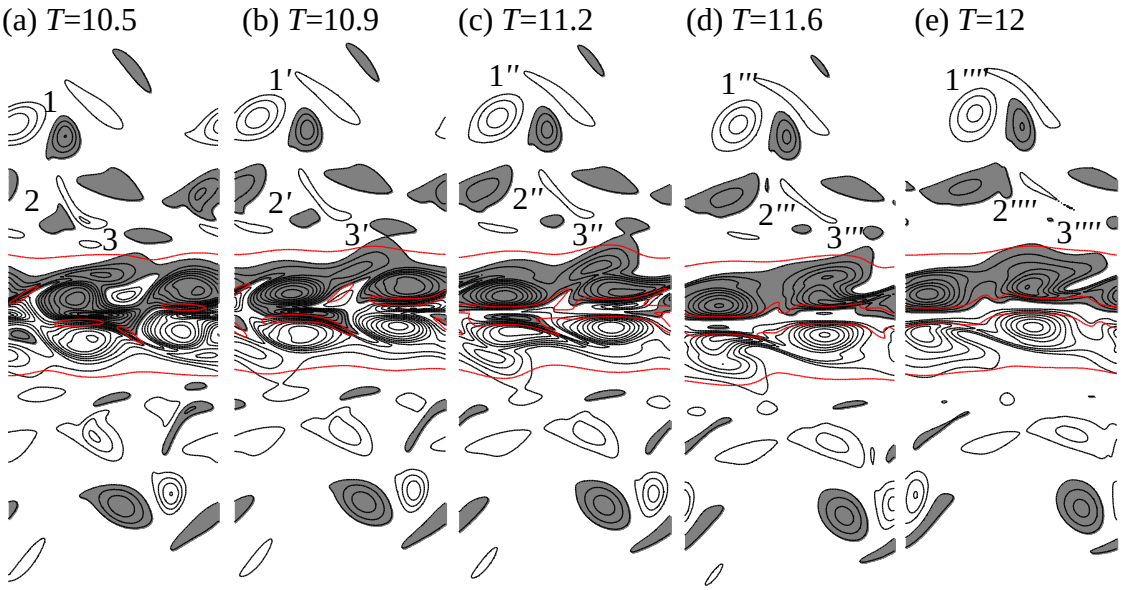

Figure 18: Meridional (z-x) plane contours of ω_y (ω_θ above the axis, $-\omega_\theta$ below the axis) before and during the regenerative growth in figure 16. Shaded regions denote negative ω_y; level are plotted at $|\omega_y|=[\omega_{min}, \omega_{max}, \delta\omega]=[0.1, 1, 0.1]$. $\Omega=0.5$ (red) indicates the core.

ω'_r of opposite sign. In summary, tilting of ω'_r into ω'_z produces ω'_z which tilts Ω_θ into amplifying ω'_r, creating a cycle of vorticity intensification. Concurrent with this intensification of ω'_r and ω'_z is tilting of ω'_r into ω'_θ without loss, resulting in continual amplification of all three vorticity components.

Examination of all three vorticity components (extrapolating ω_z from the other two) within the vortex core (marked by 3-3⁗ in figures 18(a-e) and 19(a-e)), show significant growth indicative of the effect of mean axial flow. Limitation of this growth occurs via viscous effects and the onset of core dynamics (Melander & Hussain 1994), which reduces ω'_r due to tilting of Ω_z, After growth, the intensified region (i.e., the contours marked by 3‴ in figures 18(d) and 19(d)) merges with the core fluctuations and decays (compare the two distinct regions of ω_y at 3″ in figure 18(c) to the single region at

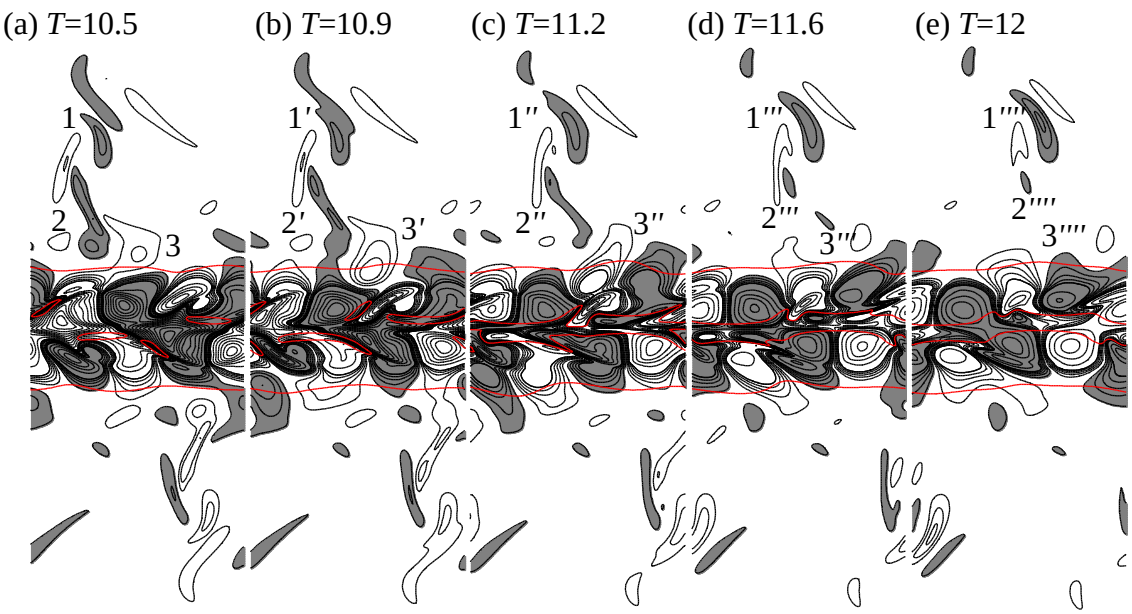

Figure 19: Meridional (z-x) plane contours of ω_x (ω_r above the axis, $-\omega_r$ below the axis) before and during regenerative growth in figure 16. Shaded regions denote negative ω_x; two level ranges are plotted, one at $|\omega_x|=[\omega_{min}, \omega_{max}, \delta\omega]=[0.02, 0.1, 0.02]$ and one at [0.1, 1.5, 0.1].

3⁗ in figure 18(e)). From analysis of the evolution of the filament's structure and the profiles of turbulent kinetic energy, the growth corresponds not to the hairpin mechanism to the mean axial strain from inviscidly generated W, suggesting that vorticity generation due to axial flow dominates the hairpin mechanism when q is in the unstable regime.

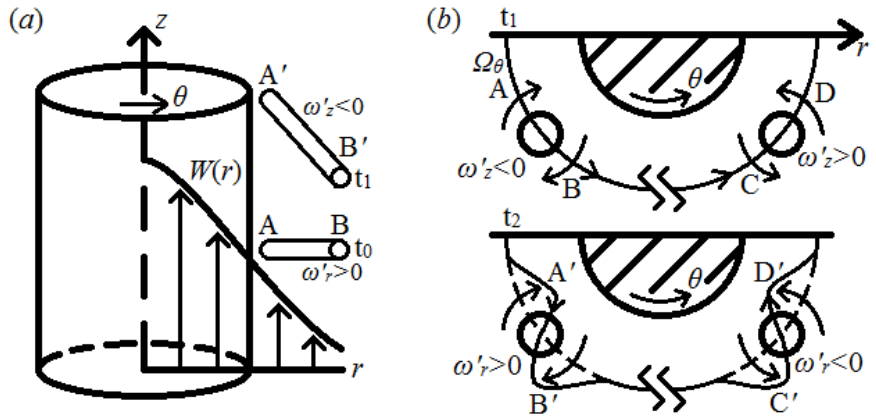

Figure 20: Vorticity generation due to (a) axial flow and (b) the related mean azimuthal vorticity (Ω_θ).

Chapter 7: Conclusion

Azimuthal vorticity filaments encircling a vortex column, generated by from a turbulent vorticity field by the mean strain rate of the vortex, undergo self-induced radial advection, resulting in the generation of axial flow within the column. Simulation results of a helical perturbation to an Oseen vortex confirms generation of axial flow and finds that at high *Re*, the vortex column becomes unstable via the *q* criterion and undergoes regenerative growth. Evolution of the vorticity field indicates that while the parent-offspring hairpin vortex mechanism scenario of HPS does generate vorticity, during the observed period of regenerative growth, the parent & offspring vortices are decaying, hence vorticity generation due to axial flow likely dominates the hairpin mechanism.

Inviscid generation of axial flow on the columnar vortex by turbulence inherently draws comparison to the viscous generation of axial flow in a viscously diffusing trailing vortex. Following Batchelor (1964), the pressure gradient due to a diffusing vortex column generates a velocity deficit in the axial flow (i.e., a decrease from the free-stream axial flow) which decreases as at $t^{-1}\log(t)$ at late times (or large downstream distances). In comparison, eqn. (9) shows that W_{tot} increases as $t^{5/2}$, while the simulation results indicate slower linear in time growth at late times. The surprising difference in late time behaviors, one decaying versus one growing, indicates the turbulence generate axial flow is more significant at late times. Furthermore, the inherent difference between a viscous and an inviscid mechanism means that the turbulence generated axial flow plays a greater role in high *Re* flows.

The analysis for azimuthally wrapped filaments can be extended to flows outside of vortex-turbulence interaction. For instance, in mixing layers, transition to turbulence (and breaking of the spanwise symmetry) occurs as the vortex sheet rolls up into spanwise vortices and then undergoes a secondary instability where streamwise vortices develop (as "ribs" on the spanwise vortices). These "ribs" are wrapped around the larger spanwise vortices similar to the azimuthally oriented vorticity filaments considered here, and would undergo similar self-induced radial advection in opposite directions. This would eventually lead to radial separation of the "ribs", generating axial flow in the larger vortex and wrapping around each other, likely leading to transition of the flow to turbulence.

Additionally, the discussed generation of axial flow is due only to the inherent structure of the filament, and thus would be present in Batchelor vortices, i.e., vortices with initial axial flow. In such a case, the generated axial flow can either lead to instability via increasing W, or can stabilize the vortex by reducing W. In a spatially evolving Batchelor vortex, like those in a lab, the generated axial flow discussed here would develop as a function of the downstream position, leading to a possible stagnation point when the generated W matches the initially present W, i.e., vortex breakdown. Furthermore, the filaments generating the axial flow would likely dictate the flow structure post-breakdown, as late time filaments are nearly axisymmetric. The conditions and parameters for breakdown have been heavily discussed for the base flow (see Leibovich 1978, Schmucker & Gersten 1988, and others); however turbulent generation of axial flow can improve prediction of vortex breakdown and potentially enable better control of breakdown.

Additionally, axial flow is known to generate perturbation growth (compare the transient growth magnitude for the Oseen vortex in PH06 to the growth for the Batchelor vortex in Heaton & Peake 2007), which means the turbulent generated axial flow also intensifies the perturbation. Physically, the radial gradient of the axial flow stretches the vorticity filaments, which counters viscous diffusion and continues the generation of *W* for longer periods. Interestingly, this presents a scenario where the filaments generate axial flow, which sustain the filament until either the filaments are destroyed by cross-annihilation, which would occur when axial self-advection of the filaments leads to dipole formation, or the vortex column transitions to turbulence.

There are three areas for future work on this topic beginning with confirming the observed trends for vortex-turbulence interaction dependent on the initial turbulence intensity. To properly assess measure these trends, higher *Re* simulations (up to Re=1 million) are needed, likely through the use of LES. Second is the regenerative perturbation growth on the vortex column, which appears to result from the axial flow reaching the unstable range. Careful examination of the flow evolution and the dynamics are needed to separate (or merge) the influence of axial velocity and the hairpin mechanism of HPS. Third is analyzing vortex breakup into turbulence due to the natural generation of axial velocity, where the mean profiles are distinctly different from the Batchelor vortex because of the region of oppositely signed mean axial velocity, necessary by the constant zero meridional circulation. Additionally, the prospect of destabilizing axial flow generated by fine scale turbulence in large scale coherent structures has applications to numerous turbulent flows where large scale structures

appear before transition to turbulence such as mixing layers, jets, wakes and boundary layers.

References

Antkowiak, A., & Brancher, P. "Transient Energy Growth for the Lamb-Oseen Vortex." *Phys. Fluids*, **16**, 1 (2004).

Antkowiak, A., & Brancher, P. "On Vortex Rings Around Vortices: an Optimal Mechanism." *J. Fluid Mech.*, **578**, 295 (2007).

Batchelor, G.K. "Axial Flow in Trailing Line Vortices." *J. Fluid Mech.*, **20**, pp 645-658 (1964).

Broderick, A., Bevilaqua, P., Crouch, J., Gregory, F., Hussain, F., Jeffers, B., Newton, D., Nguyen, D., Powell, J., Spain, A., Stone, R. & Willcox, K. "Wake Turbulence – An Obstacle to Increased Air Traffic Capacity." *National Research Council* (2008).

Callegari, A.J. & Ting, L. "Stability of Symmetric and Asymmetric Vortex Pairs Over Slender Conical Wings and Bodies." *SIAM J. Appl. Math.*, **35** pp. 148-175 (1978).

Govindaraju, S.P., & Saffman, P.G. "Flow in a Turbulent Trailing Vortex." *Physics of Fluids*, **14,** 2074 (1971).

Heaton, C. J., & Peake, N. "Transient Growth in Vortices with Axial Flow." *J. Fluid Mech.*, **587**, 271 (2007).

Hussain, A.K.M.F. "Coherent Structures and Turbulence." *J. Fluid Mech.*, **173**, pp. 303-356, (1986).

Hussain, F., Pradeep, D.S. & Stout, E. "Nonlinear Transient Growth in a Vortex Column." *J. Fluid Mech.*, **682**, pg. 304-331 (2011). Cited as HPS in text.

Hussain, F. & Stout, E. "Self-limiting and Regenerative Dynamics of Perturbation Growth on a Vortex Column" *J. Fluid Mech.*, **718**, pp 39-88 (2013). Cited as HS in text.

Kerswell, R. "Elliptical Instability." *Ann. Rev. of Fluid Mech.*, **34**, pp. 83-113 (2002).

Leibovich, S. "The Structure of Vortex Breakdown." *Ann. Rev. of Fluid Mech.*, **10**, pp. 221-246 (1978).

Lessen, M., Singh, P., & Paillet, F. "The Stability of a Trailing Line Vortex. Part 1. Inviscid Theory." *J. Fluid Mech.*, **63**, pp 753-763 (1974).

Melander, M. V., & Hussain, F. "Polarized Vorticity Dynamics on a Vortex Column." Physics of Fluids A **5** (8) pp. 1992-2003 (1993).

Melander, M.V., & Hussain, F. "Core Dynamics on a Vortex Column." *Fluid Dyn. Res.*, **13**, 1 (1994).

Morkovin, M. "Critical Evaluation of Transition from Laminar to Turbulent Shear Layers with Emphasis on Hypersonically Traveling Bodies." Technical Report AFFDL-Tr-68-149 (1969).

Pradeep, D.S., & Hussain, F. "Effects of Boundary Condition in Numerical Simulations of Vortex Dynamics." *J. Fluid Mech.*, **516,** 115 (2004). Cited as PH04 in text.

Pradeep, D.S., & Hussain, F. "Transient Growth of Perturbations in a Vortex Column." *J. Fluid Mech.*, **550,** 251 (2006). Cited as PH06 in text.

Pradeep, D.S., & Hussain, F. "Vortex Dynamics of Turbulence-Coherent Structure Interaction." *Theoretical and Computational Fluid Dynamics*, **24,** 265 (2010). Cited as PH10 in text.

Schmucker & Gersten "Vortex Breakdown and its Control on Delta Wings," *Fluid Dyn. Res.*, **3**, 268 (1988).

Schoppa, W., & Hussain, F. "Coherent Structure Generation in Near-wall Turbulence." *J. Fluid Mech.*, **453**, pp. 57-108 (2002).

Spalart, P. "Aircraft Trailing Vortices." *Annual Review of Fluid Mechanics* **30**, 107 (1998).

Stewartson, K. & Brown, S. "Near-neutral Center-modes as Inviscid Perturbations to a Trailing Line Vortex." *J. Fluid Mech.*, **156**, pp. 387-399 (1985).

Ting, L. & Klein, R. *Viscous Vortex Flows*. Springer-Verlag, Berlin Heidelberg New York (1991).